Atmospheric Pollution Research xxx (xxxx) xxx–xxx

HOSTED BY

ELSEVIER

Contents lists available at ScienceDirect

Atmospheric Pollution Research

journal homepage: www.elsevier.com/locate/apr

Simulation of summer ozone and its sensitivity to emission changes in China

Hao Guo[a,*], Kaiyu Chen[a], Pengfei Wang[a], Jianlin Hu[b], Qi Ying[c], Aifang Gao[d,e], Hongliang Zhang[a,f,**]

[a] Department of Civil and Environmental Engineering, Louisiana State University, Baton Rouge LA, 70803, USA
[b] Jiangsu Key Laboratory of Atmospheric Environment Monitoring and Pollution Control, Jiangsu Engineering Technology Research Center of Environmental Cleaning Materials, Collaborative Innovation Center of Atmospheric Environment and Equipment Technology, School of Environmental Science and Engineering, Nanjing University of Information Science & Technology, 219 Ningliu Road, Nanjing, 210044, China
[c] Zachry Department of Civil Engineering, Texas A&M University, College Station, TX, 77843, USA
[d] School of Water Resources and Environment, Hebei GEO University, Shijiazhuang, Hebei Province, 050031, China
[e] Hebei Key Laboratory of Sustained Utilization and Development of Water Resources, Shijiazhuang, Hebei Province, 050031, China
[f] Department of Environmental Science and Engineering, Fudan University, Shanghai, 200433, China

ARTICLE INFO

Keywords:
Ozone
Isopleth
Sensitivity
CMAQ
China

ABSTRACT

Rapid economic growth and associated emission increase in China have led to severe air pollution in recent decades. As fine particulate matter concentration is decreasing due to strict control measures, ozone (O_3) concentration has an increasing trend with adverse effects on human health and ecosystems. In this study, the Community Multi-scale Air Quality (CMAQ) model was used to investigate the formation of O_3 in China during three high concentration episodes in summer 2013 and analyzed its sensitivity to emission changes. Compared with observation data, O_3 performance met the EPA criteria of mean normalized bias (MNB) within ± 0.15 in major parts of China including five megacities. The diurnal variation of O_3 had similar trend with temperature. The August episode (6–12) had the highest daily maximum 1-h O_3 of ~100 ppb in North China Plain (NCP), while the July episode (11–19) had the lowest concentrations of ~50 ppb. The O_3 production rates (OPR) were higher at NCP and the Yangzi River Delta (YRD), but O_3 production efficiencies (OPE) acted in contrary. O_3 isopleth showed that NOx controlled O_3 concentration in most areas of China. Reducing VOC would have minor effects on O_3 concentrations while reducing NOx could largely reduce O_3 concentration except for urban areas such as Shanghai and Guangzhou. Linear correlations were observed between secondary organic aerosol (SOA) and O_x ($O_3 + NO_2$) concentrations in August at Shanghai and Guangzhou, indicating correlations between O_3 and other photochemical compounds. This study provides valuable information for designing effective control strategies for O_3 in China.

1. Introduction

Atmospheric pollution has been severe in recent decades in China due to the increase of industries, population, and urbanization. Among different air pollutants, ozone (O_3) is secondarily formed in photochemical reactions of nitrogen oxides (NOx) and volatile organic compounds (VOCs) with the existence of sunlight, and it is adverse to human health and ecosystems (WHO, 2006). China started to publish real-time concentration of six criteria pollutants (carbon monoxide, lead, nitrogen dioxide, O_3, particulate matter, and sulfur dioxide) from the ambient air quality monitoring networks since 2013 (Sun et al., 2014) after several extreme air pollution events occurred in past 10 years (Guo et al., 2017; Wang et al., 2014b). However, the monitoring system only includes criteria pollutants and the precursors of O_3 production such as VOCs, which are important to understand the sources of air pollution and form effective O_3 concentration controls, are not measured. The limited information of detailed chemical composition of air pollutants narrows our capability to investigate the formation mechanisms of O_3. Also, the majority of observation sites are located in urban areas but suburban and rural regions also have large population and experience high concentrations of air pollutants, especially O_3 (Wen et al., 2015).

As a complement to observational analysis, chemical transport models (CTMs) are often used to understand the formation and

Peer review under responsibility of Turkish National Committee for Air Pollution Research and Control.
* Corresponding author.
** Corresponding author. Department of Civil and Environmental Engineering, Louisiana State University, Baton Rouge LA 70803, USA.
E-mail addresses: hguo8@lsu.edu (H. Guo), hlzhang@lsu.edu (H. Zhang).

https://doi.org/10.1016/j.apr.2019.05.003
Received 23 October 2018; Received in revised form 6 May 2019; Accepted 6 May 2019

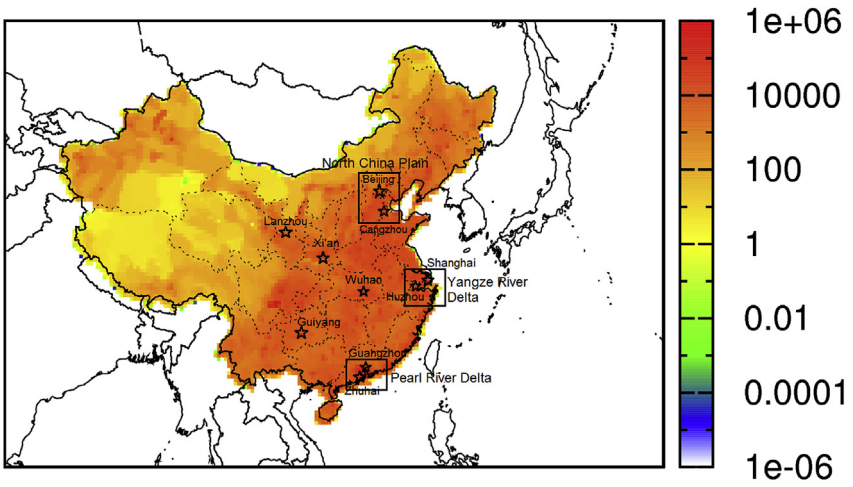

Fig. 1. Model domain and population density distribution (numbers per grid in log scale).

Table 1
Meteorology performance in summer 2013 (OBS, mean observation; PRE, mean prediction; MB, mean bias; GE, gross error; and RMSE, root mean square error).

Averaged values	Statistics	June	July	August	Benchmarks[a]
T (°C)	PRE	28.3	29.0	30.5	
	OBS	26.9	28.0	29.7	
	MB	1.4	1.0	0.8	≤ ± 0.5
	GE	2.7	1.5	1.3	≤2.0
	RMSE	3.2	1.8	2.0	
WS (m/s)	PRE	3.2	3.1	3.1	
	OBS	3.0	2.9	2.8	
	MB	0.1	0.2	0.2	≤ ± 0.5
	GE	1.3	2.0	2.4	≤2.0
	RMSE	1.5	2.4	2.8	≤2.0
WD (°)	PRE	167.0	165.9	187.3	
	OBS	162.9	171.5	183.3	
	MB	4.1	−5.6	4.0	≤ ± 10
	GE	16.4	25.1	18.9	≤ ± 30
	RMSE	36.5	46.8	42.3	
RH (%)	PRE	57.1	69.6	63.7	
	OBS	65.3	74.8	67.5	
	MB	−8.1	−5.2	−3.8	
	GE	15.2	10.8	8.6	
	RMSE	20.6	25.7	18.6	

Note.
[a] Are benchmarks limits suggested by Emery et al. (2001).

transport of pollutants, predict future air pollution events, and provide high temporal and spatial resolution data for epidemiological studies. Hu et al. (2016) studied the temporal and spatial characteristics of some important pollutants like $PM_{2.5}$ and O_3 concentration of China in 2013 using the Weather Research and Forecasting and Community Multi-scale Air Quality (WRF/CMAQ) modeling system based on a modified gas phase photochemical mechanism. WRF/CMAQ modeling was utilized to predict the impact of emission control strategies and weather conditions on O_3 haze pollution in Zhongshan, Guangdong, China (Mai et al., 2016). Zhao et al. (2016) found that intermediate-volatility emissions together increase photochemical pollutants concentrations in Eastern China by about 40%. However, few of these studies concentrate on a certain O_3 episode to dig into the concentration variation in a short period like one week and analyze high concentration events for different regions.

Many studies focused on the contributions of different precursors from various sources to O_3 concentration. Shao et al. (2009) found O_3 concentration in Pearl River Delta slightly decreased due to stringent nitrogen oxide (NOx) emission controls between 1995 and 1996. Based on temporal and spatial variations of VOC mixing ratios, Wei et al. (2014) found photochemical reactions were more intensive around the refinery to produce O_3 at rural area of Beijing in summer 2011. Wang et al. (2014a) found that O_3 weekend effect (OWE) in the metropolitan area of Beijing–Tianjin–Hebei (BTH) was due to the weekly variation of NOx concentration.

Although lots of studies discovered the contributions of different O_3 precursors, the sensitivity of O_3 to NOx and VOCs emission changes is required for designing effective O_3 control strategies. Tonnesen and Dennis (2000) indicated that further evaluations using modeling studies, measurements, and test cases with NOx or VOCs emissions changes are needed to determine how reliably they distinguish NOx- and radical-limited conditions. Jiang et al. (1997) found that reduction in a lumped class of aromatics emissions alone could achieve significant O_3 reduction in the Lower Fraser Valley (LFV) of British Columbia, Canada and any overestimation of NOx or underestimation of VOCs in emission inventory could cause underestimation of O_3 by photochemical models. Cohan et al. (2005) conducted a modeling study for a high O_3 episode in the southeastern United States with a second-order direct sensitivity method and explored the nonlinear responses of O_3 to emissions of its precursors. Although sensitivity studies were conducted in North American, rare studies have been done for China.

In this study, WRF/CMAQ modeling system was used to simulate detailed temporal and spatial distribution of photochemical pollutants of three one-week long episodes in June, July and August 2013 in China. The modeling results were validated based observation data obtained from the Chinese Ministry of Environmental Protection (MEP, 2012). The temporal and spatial variations of photochemical pollutants were analyzed. O_3 isopleths analysis were conducted to investigate the sensitivity of O_3 concentrations to changes in NOx and VOCs emissions and, which helps to design effective emission control strategies to reduce O_3 concentrations at different locations. The correlations of SOA and Ox concentration were also examined.

2. Method

2.1. Model improvement

The CMAQ v5.0.2 model system developed by the U.S. EPA Atmospheric Science Modeling Division was used in this study. The original model was modified to apply a more detailed SAPRC-11 photochemical mechanism with more adequate processes of isoprene oxidation chemistry pathways to generate SOA from surface controlled reactive uptake of dicarbonyls, isoprene epoxydiol (IEPOX) and methacrylic acid epoxide (MAE) (Ying et al., 2015) as well as in-cloud processing of isoprene oxidation products glyoxal (GLY) and methylglyoxal (MGLY) (Ervens and Volkamer, 2010; Volkamer et al., 2007). Detailed information of the modified mechanism and model can be

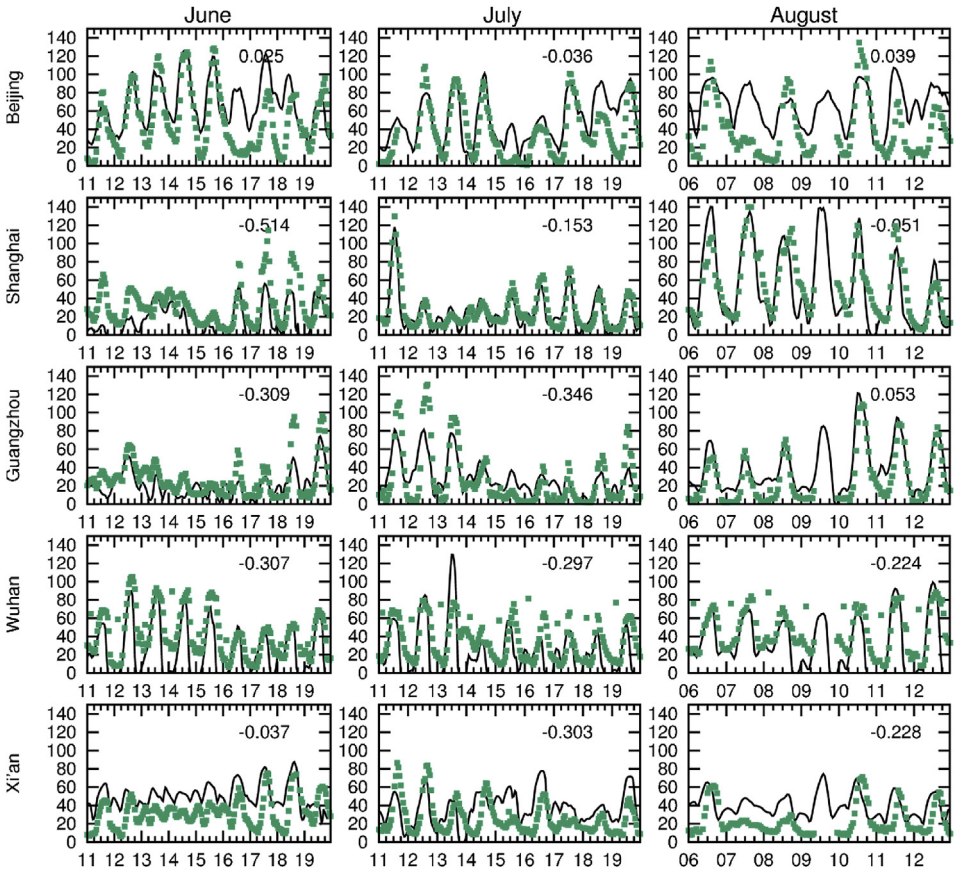

Fig. 2. Time series of hourly O_3 concentrations in five megacities during summer episodes in 2013 (Green dot represents observation data, solid line shows prediction and NMB value is shown on upper-right corner, 6 a.m. to 5 p.m. are day hours, units are ppb for O_3 concentrations). (For interpretation of the references to colour in this figure legend, the reader is referred to the Web version of this article.)

found in Ying et al. (2015). This improved CMAQ model had been applied to analyze O_3 and SOA formation in Eastern US (Ying et al., 2015) to determine contributions of isoprene to summertime ambient SOA concentrations. The original SOA yields for toluene and xylene under high NOx concentrations in the model were replaced with the higher toluene values (Li et al., 2015; Ying et al., 2015). The updated mechanism had been applied in Mexico City (Karambelas et al., 2014) and reduced the negative bias reported in previous studies (Li and Rappenglück, 2014; Zhang et al., 2014).

2.2. Model application

In this study, a 36 km horizontal resolution domain that covers China and surrounding countries in East Asia were applied as shown in Fig. 1. Fig. S1 shows the monitoring sites for meteorology and air quality data. Topography distribution is shown in Fig. S2. There were 18 layers with surface layer thickness of 35 m and the overall model height of 20 km. The Weather Research & Forecasting model (WRF) v3.7.1 was utilized to generate meteorology inputs with initial and boundary conditions from FNL (Final) Operational Global Analysis data National Center for Atmospheric Research, which is available on $1.0 \times 1.0^{\circ}$ grids continuously for every 6 h (http://dss.ucar.edu/datasets/ds083.2/). The outputs of WRF were processed by Meteorology-Chemistry Interface Processor (MCIP) v4.2 to generate CMAQ inputs. The meteorology observation data to validate WRF performance were obtained from National Climate Data Center (NCDC) website. Initial and boundary conditions were set to CMAQ default values.

Anthropogenic emissions were generated based on the Multi-resolution Emission Inventory for China (MEIC) developed by Tsinghua University (http://www.meicmodel.org). MEIC (V1.0) is a new version emission inventory in China improved several emission sources such as a unit-based emission inventory for power plants (Wang et al., 2012) and cement plants (Lei et al., 2011), a high-resolution county-level vehicle emission inventory (Zheng et al., 2014), a non-methane VOC mapping approach for different chemical mechanisms (Li et al., 2014). The wild fire emission was taken from the Fire Inventory from NCAR (FINN) (Wiedinmyer et al., 2011). Biogenic emissions were generated using the Model for Emissions of Gases and Aerosols from Nature (MEGAN) v2.1 (Guenther et al., 2012). Three episodes in summer 2013 with peak O_3 concentrations at different regions of China were selected: June 11–19, July 11–19 and August 6–12. O_3 observation data in 59 cities were obtained from the official website of China National Environmental Monitoring Center to validate the model simulation.

2.3. Ozone production rate (OPR) and ozone production efficiency (OPE)

In evaluating the O_3 production, two commonly used O_3 metrics of O_3 production rate (OPR) and O_3 production efficiency (OPE) were applied. Since NO_2 photolysis is the major reaction to form O_3 in the ground level (Crutzen, 1971), OPR (ppb/hour) is equivalent to the formation rate of NO_2 via two production pathways: the reaction of HO_2 with NO and the reactions of organic peroxy radical (RO_2) with NO as in Eq. (1).

$$OPR = k_{HO2+NO}\,[HO_2][NO] + k_{RO2+NO}\,[RO_2][NO] \quad (1)$$

OPE describes the number of molecules of O_3 generated per molecule of NOx oxidized into reactive nitrogen species (e.g., HNO_3) and can be calculated using Eqs. (2) and (3).

$$OPE = OP_{R/L(NOx)} \quad (2)$$

$$L(NOx) = k_{OH+NO2}\,[OH][NO_2] \quad (3)$$

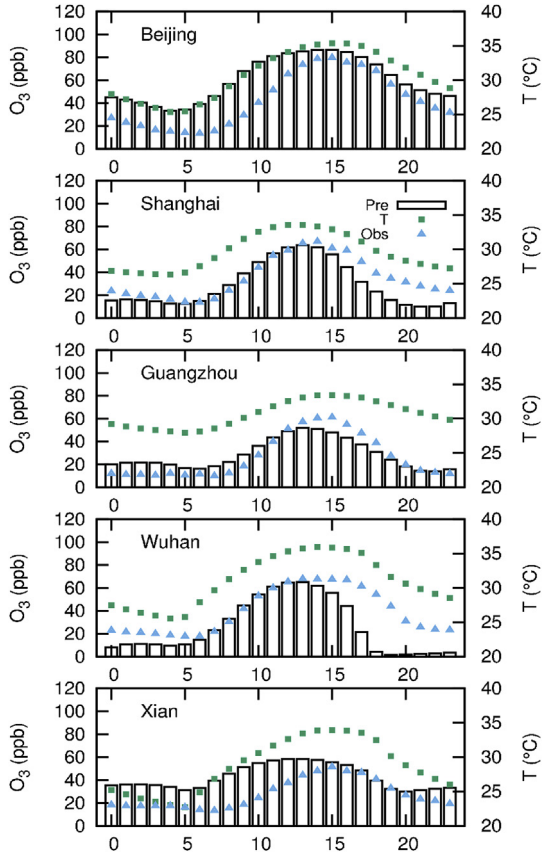

Fig. 3. Average diurnal variation of O_3 concentration in five megacities (Green dot represent temperature, blue triangle stands for observation of O_3 concentrations and histogram shows prediction of O_3 concentrations). (For interpretation of the references to colour in this figure legend, the reader is referred to the Web version of this article.)

3. Results

3.1. Meteorology validation

Meteorology plays important role in predicting the transportation, formation and deposition of atmospheric pollutants. Model performance varies for different study areas, time periods, and domain settings. To ensure the accuracy of CMAQ simulation, the meteorology inputs from WRF were validated against observational data at all available sites (~1200 sites) within the domain as shown in Fig. 1. The data were downloaded from the National Climate Data Center (NCDC) and the parameters included temperature (T) and relative humidity (RH) at 2 m above surface, and wind speed (WS) and wind direction (WD) at 10 m above surface. The daily average values were calculated only when there were more than 20-h valid data for each day. Details on the treatment of the observation values can be found in several previous studies (Hu et al., 2014; Wang et al., 2014b).

Table 1 and Table S1 shows the overall and city-wise model performance statistics of mean observation (OBS), mean prediction (PRE), mean bias (MB), gross error (GE) and root mean square error (RMSE) based on the observations and WRF predictions with criteria suggested by previous studies (Emery et al., 2012). The WRF model predicts slightly lower temperature than observations in the three summer episodes. GE values are generally within the suggest value of 2.0 °C. MB values are always larger than 0.5 °C. GE values for WS mostly meet the suggested values of 2.0 m/s except the GE value of August episode, same as MB values. The RMSE values at July and August are slightly higher than the criteria. GE and MB values of WD are all within the criteria of ± 30° and ± 10°. RH is generally underestimated in the study episodes with the MB of −8.1%~-3.8%. Compared with other similar modeling works based on WRF (Borge et al., 2008; Mohan and Bhati, 2011; Zhang et al., 2014), the WRF model performance is acceptable although the resolution and study area vary from one study to another.

3.2. Model performance of O_3

The performance of O_3 is validated by comparing the prediction with hourly observation from China National Environmental Monitoring Center (http://113.108.142.147:20035/emcpublish/) as shown in Fig. S1. If multiple sites are located at same city, the averaged values were used. Credibility check on the dataset was used to exclude invalid data point and avoided problematic data points before calculation. The daily average pollutant concentrations were calculated only when there were more than 20-h valid data for each day. Details on the treatment of the observation values can be found in several previous studies (Hu et al., 2014; Wang et al., 2014b).

Temporal variations of O_3 concentrations in three summer episodes are shown in Fig. 2. Model simulation correctly reproduced the O_3 concentration variation in the selected week-long episode compared with observation data. In all the five megacities, model captured most of the peak O_3 concentration in the episode as shown in the figure. In Beijing, the small NMB value at up-right corner indicates a nice modeling performance. The underestimation is observed at June episode of simulation in Shanghai, Guangzhou and July, August episode in Xi'an. The NMB values of Wuhan simulation in all three episodes exceed the EPA criteria. WRF results generally shows an over-estimation of temperature in five selected cities as in Table S1, so the underestimation of O_3 concentration may due to uncertainties in emission inventory.

Fig. 3 shows diurnal variation of model prediction with observed O_3 concentration and temperature at the five mega cities including Beijing, Shanghai, Guangzhou, Wuhan and Xi'an. The periodical variation that O_3 concentration increases with the existence of sunshine in the morning and decreases with sunset at night can be observed in the figure. The diurnal variation of O_3 shows a similar trend with the temperature. Generally, the O_3 concentration varies with the temperature during day and night in Fig. 3 since the sunshine is the

Table 2
Model performance on O_3-8 h concentration in different regions during summer 2013. (NMB: normalized mean bias; NME: normalized mean error; and AUP: accuracy of unpaired peak).

		North	Northeast	Northwest	Central	East	South	Southwest
NMB	June	−0.007	−0.047	−0.179	−0.231	−0.252	−0.341	−0.032
	July	−0.013	−0.215	−0.151	−0.253	−0.123	−0.360	−0.179
	August	0.033	−0.047	−0.258	−0.058	−0.112	−0.006	−0.206
NME	June	0.197	0.189	0.263	0.307	0.306	0.341	0.181
	July	0.143	0.265	0.176	0.420	0.243	0.357	0.254
	August	0.219	0.261	0.275	0.251	0.297	0.142	0.275
AUP	June	0.013	0.034	0.052	0.055	0.016	0.010	0.031
	July	0.048	0.122	0.025	−0.023	0.021	0.024	0.018
	August	0.038	0.065	0.096	0.084	0.113	0.078	0.036

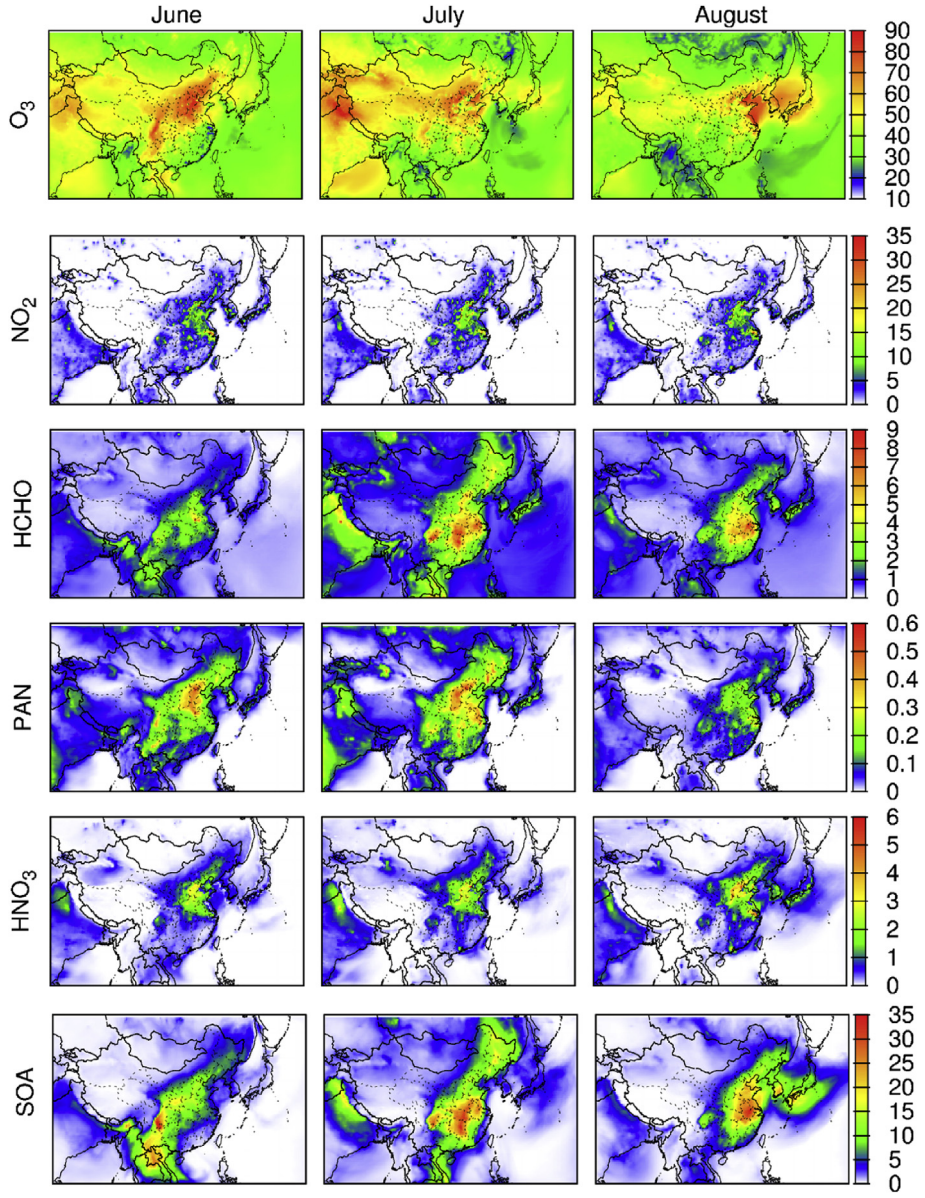

Fig. 4. Predicted regional distribution of O_3, NO_2, HCHO, PAN, HNO_3, and SOA in the summer episodes (Units are in ppb except SOA is in $\mu g/m^3$).

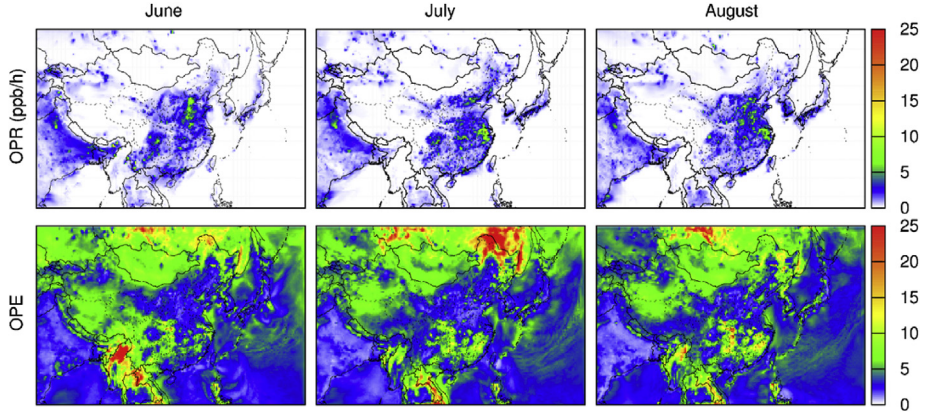

Fig. 5. Predicted ozone production rate (OPR, unit is ppb per hour) and ozone production efficiency (OPE) in high O_3 hours (11 a.m.–6 p.m.) at summer episodes.

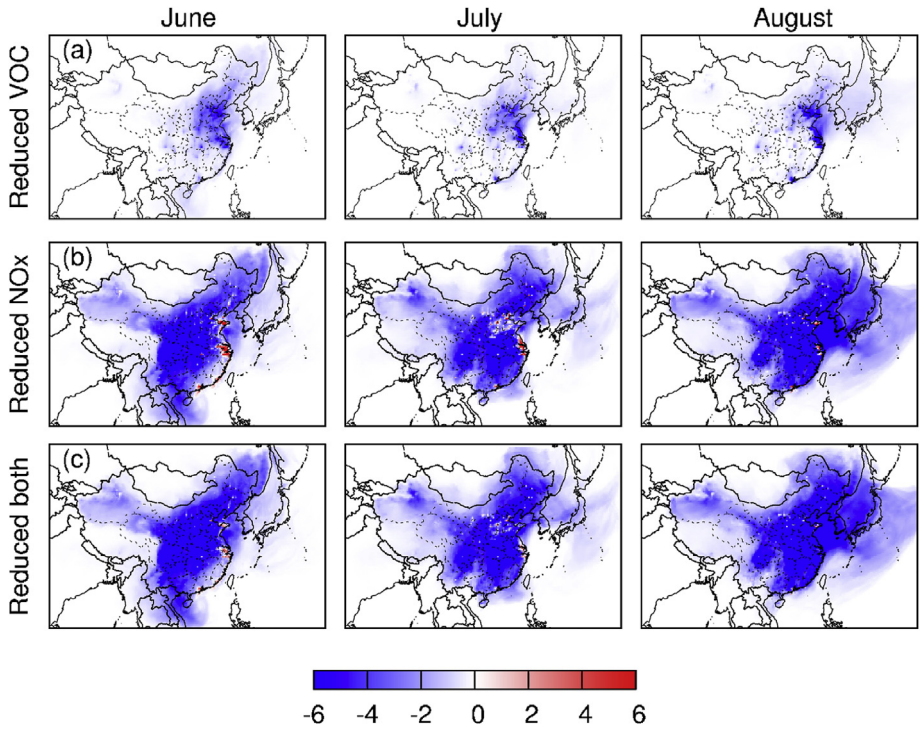

Fig. 6. Regional changes in O_3 concentrations by reducing 40% VOCs (a) and 40% NOx (b) and 40% of both anthropogenic VOCs and NOx (c) (Units are ppb).

required photochemical condition in O_3 formation and temperature also influence the process to form O_3 (Jenkin and Clemitshaw, 2000). In Beijing, Shanghai and Guangzhou, the diurnal variation plot shows our predictions are close to the observation value. It is also noticed that Beijing exhibit more substantial diurnal variations and higher diurnal O_3 concentrations than the rest cities. The daily maximum 1-h O_3 varies small at Xi'an, which has lowest diurnal O_3 concentration value and overestimation occurs. On the contrary, prediction in Wuhan underpredict the O_3 concentration after sunset hour 5 p.m. in afternoon.

As the emissions, topography and meteorology vary significantly over China, the model performance is also examined based different regions. Table 2 shows the model performance statistics of 8 h peak O_3 (O_3-8 h) in different regions of China. Normalized Mean Bias (NMB), Normalized Mean Error (NME) and Accuracy of Unpaired Peak (AUP) values are calculated to evaluate our model performance for three summer episode with the suggest cut off value of 60 ppb (considering the monitoring sites are almost urban) towards O_3 concentration by US EPA, and then compared with US EPA criteria of NMB (within ± 0.15), NME (≤0.30) and AUP (within ± 0.20). In North, Northeast and East China, NMB, NME and AUP values are all within the EPA criteria in episodes of June, July and August. The slight underestimation is found on Northwest and Southwest China simulation as the NMB value slightly higher than criteria. In Central and South China, the underestimation occurs at episode of June and July since the NMB values higher than EPA criteria, but the model performance on August is within criteria. As the monitoring sites are more sufficient in North and East China to represent the whole area, the validation result is more convictive in these areas.

3.3. Spatial and temporal variations of O_3

Spatial distribution of O_3 concentrations is shown in Fig. 4. Different from other species, O_3 concentrations are higher in June and August. In episode at June, the extreme O_3 events occurs at NCP and Sichuan Basin and the O_3 concentration reaches 100 ppb. The O_3 concentration become lower ~70 ppb in July at NCP and 50 ppb in Sichuan Basin. In August, the YRD and NCP both suffer extreme high O_3 concentration for 100 ppb.

All the species in Fig. 4 have a higher concentration in more industrialized and population aggregated area. SOA has a concentration of 35 μg/m^3 at Sichuan Basin in June and Central China, Yangzi River Delta (YRD) suffered most at July and August episodes. NO_2 concentration is as high as 35 ppb in some regions, especially area with high population density like NCP, YRD and Pearl River Delta (PRD). The high vehicle emission could be the main reason for the high concentration of NO_2 in these areas (Chan and Yao, 2008). NO_2 concentration shows some spatial concentrations in June, July and August in major parts of China. As the termination species of NOx reaction cycle, the spatial distribution of HNO_3 concentration is very similar to NO_2 concentration in three episodes and HNO_3 concentration can be as high as 6 ppb. HCHO concentration is higher in July and Central China (9 ppb), YRD suffers the most in August. Unlike HCHO, PAN concentration is higher in June and July at NCP (0.6 ppb).

Fig. 4 also shows the spatial variation of species related to photochemical processes in the atmosphere. NO_2 directly involves in photochemical reactions to generate NO and active oxygen radical, which can react with oxygen molecule to form O_3. HCHO can be photolyzed with existence of oxygen to produce HO_2, which converts NO back to NO_2 without consuming O_3 and leads to O_3 accumulation in the atmosphere. PAN is also an important species as secondary pollutants. Hydrocarbons react with oxygen and NO_2 with the existing of sunlight to form PAN in atmosphere. It is a good indicator to determine the VOCs sources are anthropogenic or biogenic. At last, HNO_3 is the termination products of NO_2 reaction at nighttime. NO_2 is oxidized by O_3 to form NO_3 and NO_3 react with NO_2 to generate N_2O_5, which can react with H_2O to finally form HNO_3.

Fig. 5 shows OPRs and OPEs results based on prediction gas phase species concentrations in high O_3 hours (11 a.m.–6 p.m.). In severe O_3 polluted area like NCP and YRD, OPR can be as high as 10 ppb/h in daytime, which indicate a rapid increase in O_3 concentration in these regions at daytime. On the contrary, OPE values are found to be very low in these regions since OPEs qualitatively have an inverse dependence on NOx concentrations. In high NOx urban areas, OPE was found to have a low value of 2–4. This phenomenon is more obvious at July

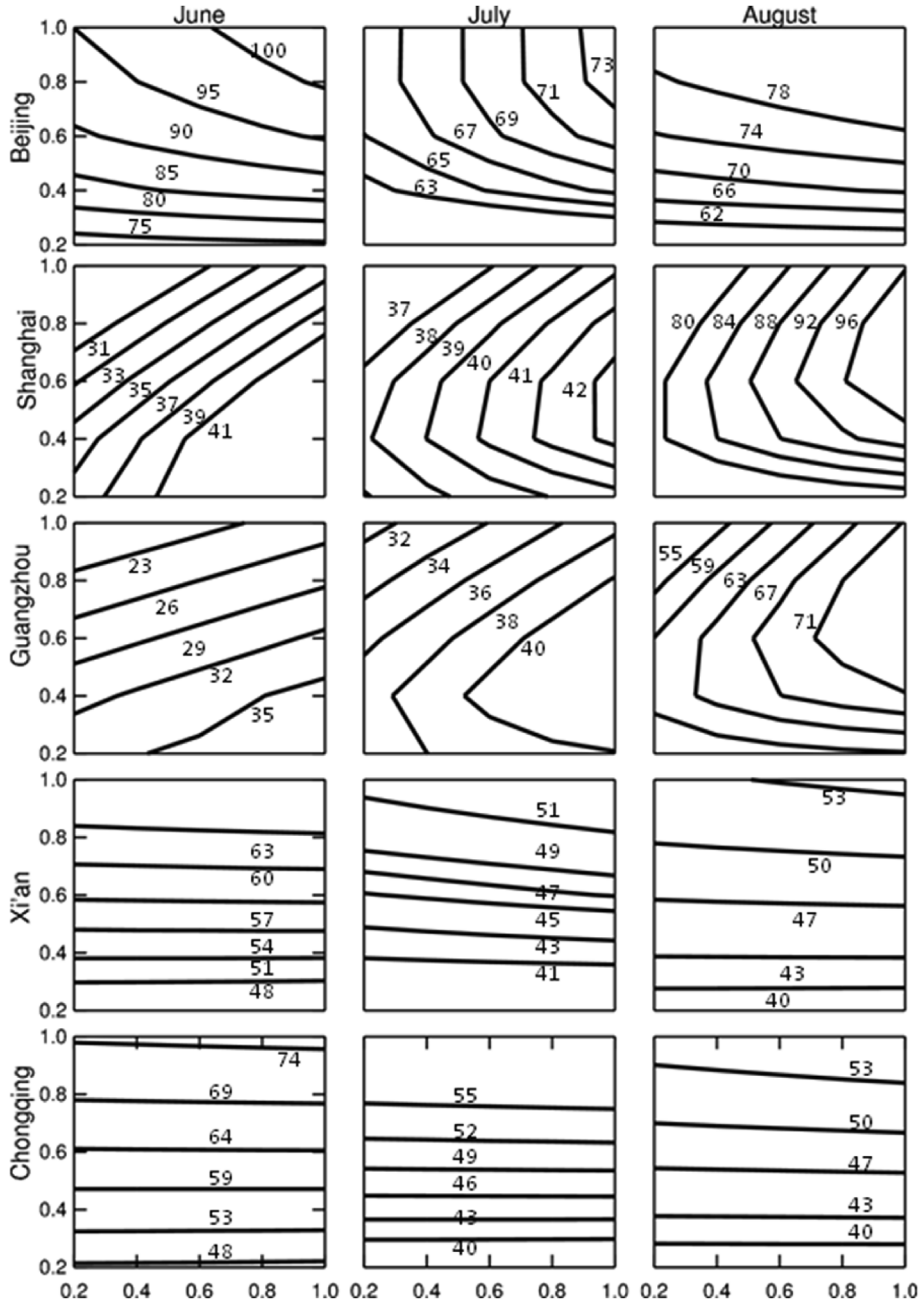

Fig. 7. O_3 isopleth at five megacities in summer episodes of China (x axis shows ratio of VOC emissions and y axis shows ratio of NOx emissions. Unit of O_3 is ppb). The same for Fig. 7.

2013 since the NOx concentration is higher compared to June and August in Fig. 3.

3.4. Isopleth of O_3

Isopleth is a two-dimensional plot showing the dependence of concentrations of atmospheric pollutants on changing conditions due to nonlinear reactions (Paulot et al., 2009). In isopleths, the contour line indicated a constant O_3 concentration under different combinations of reductions of VOCs and NOx in a single location. For example, O_3 isopleth is usually used to check the change of maximum O_3 concentration due to changing anthropogenic emissions of anthropogenic NOx and VOCs. To examine the impact toward O_3 concentrations caused by reduction of NOx and VOCs emissions, the O_3 isopleths were constructed. Anthropogenic NOx and VOCs emissions were reduced by 20%, 40%, 60%, and 80%, and simulation was conducted for each combination of NOx and VOCs to generate the isopleth plots for O_3.

Fig. 6 shows regional plot of the O_3 prediction with 40% reduction of NOx and VOCs. From the comparison of based case with reduced NOx case in Fig. 5, the O_3 concentration can decrease 4–6 ppb in major parts of China when reduced 40% of NOx emission, but controlling VOCs, which only reduce the O_3 concentration at the region of North China and Yangzi River Delta, have less effect on reduction of O_3 concentration compared with NOx. On the contrary of major parts of China, VOCs controls O_3 concentration in some regions at Yangzi River Delta and Shandong Peninsula as red area in the reduced NOx figure indicate the O_3 concentration increase 2–6 ppb with the reduced NOx concentration.

The detailed O_3 isopleth plot in Fig. 7 brings more information in five megacities form different region of China: Beijing, Shanghai,

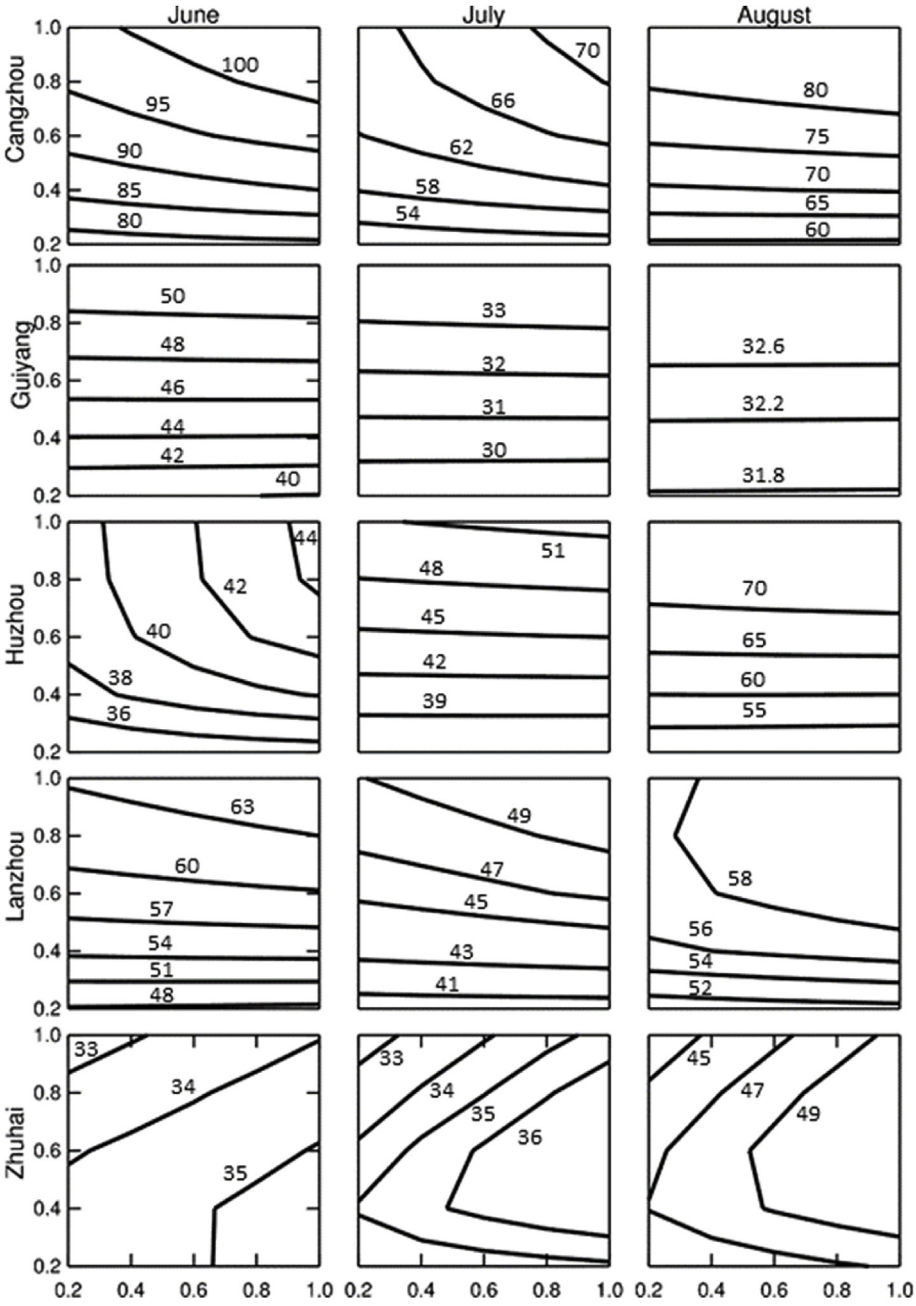

Fig. 8. O_3 isopleth at five suburban cities in summer episodes of China.

Guangzhou, Xi'an and Chongqing. The isopleth plots show minor change in three summer episodes. In isopleth plot of Beijing, Xi'an and Chongqing, these cities located in NOx controlling zone, which indicated that reducing VOCs has minor effects on O_3 concentrations with the contour line (indicate O_3 concentration) parallel to the X axis (indicate ratio to original VOCs concentration), while reducing NOx can largely reduce O_3 concentration. For example, in O_3 isopleth of Chongqing at June, the O_3 concentration dropped from 69 to 64 ppb when NOx ratio decreased from 0.8 to 0.6 at VOCs ratio of 0.6. Different from the isopleth at Beijing, Xi'an and Chongqing, the isopleth plot at Shanghai and Guangzhou shows both VOCs and NOx contribute to the O_3 formation and controlling strategy should be chosen based on corresponding location of O_3 concentration in the isopleth. Compared with megacities, the O_3 isopleth plot in sub-urban areas shows similar pattern in Fig. 8. In isopleth plots of Cangzhou (located at NCP), Guiyang (located at Southwest China), Huzhou (located at YRD) and Lanzhou (located at Northwest China), these cities located in NOx controlling zone. Isopleth plot of Zhuhai (located at PRD) shows both VOCs and NOx contribute to the O_3 formation. In conclusion, the O_3 control strategies in different regions should be different based on its sensitivity to changes in NOx and VOCs emissions.

3.5. SOA–Ox relationships

The SOA and Ox concentrations are expected to be linear correlated if they are formed on similar timescales and at the same location as they are both formed from VOCs oxidation. This correlation between SOA and Ox has been reported in variety of previous experimental and modeling studies (Wood et al., 2010; Zhang and Ying, 2011). Fig. 9 shows correlations between the SOA and Ox concentrations at five megacities during three summer episode of June, July and August. In August of Shanghai and Guangzhou, the slope of a linear fit (ΔSOA/

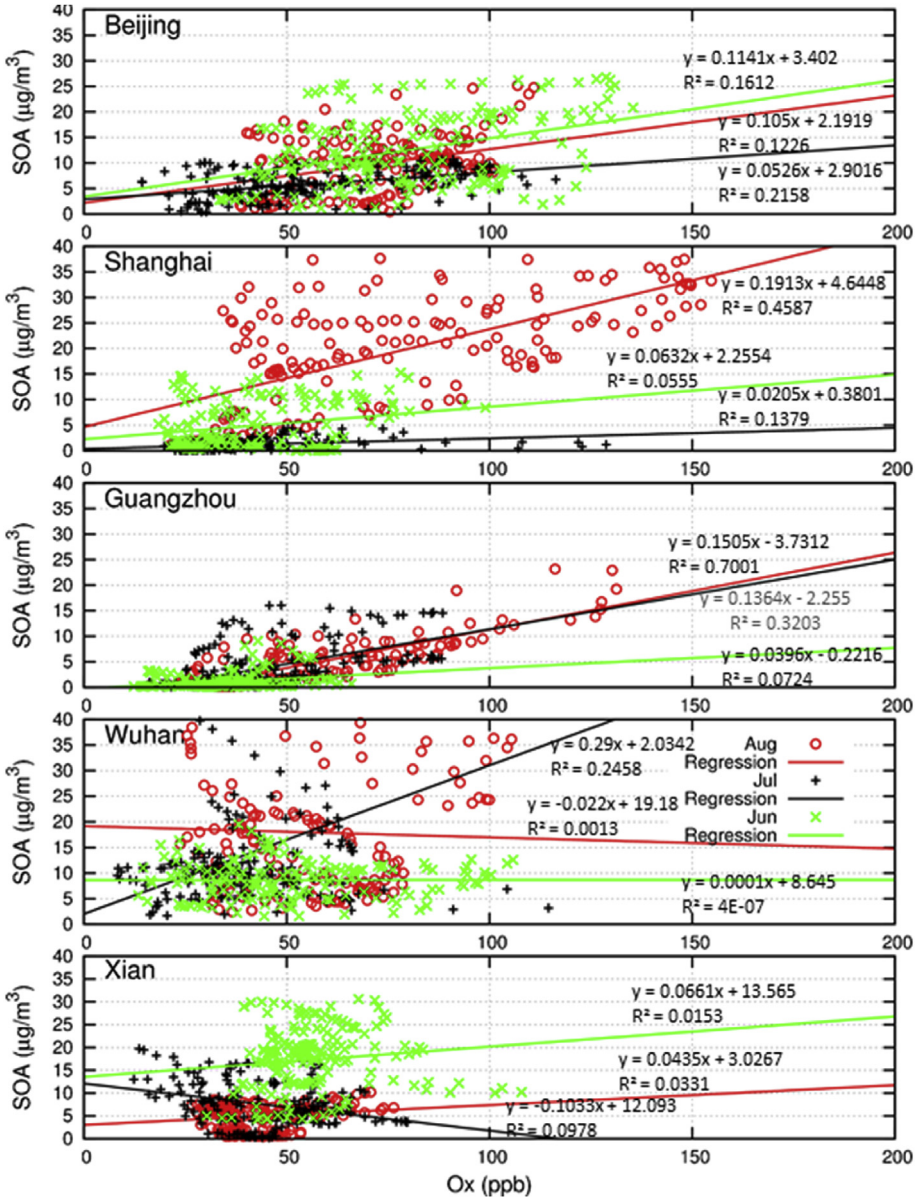

Fig. 9. Relationships between SOA and Ox (O_3+NO_2) concentrations at five megacities in China. Regression equation is shown around the trend line. (Green dots and line indicate June results, black dots and line indicate July results, red dots and line indicate August results). (For interpretation of the references to colour in this figure legend, the reader is referred to the Web version of this article.)

ΔOx) is 0.191 and 0.151 μg m^{-3} SOA/ppb Ox with R^2 value of 0.459 and 0.700, respectively. This correlation may indicate that Ox and SOA are from the similar sources and produced from local VOCs oxidation. There is no observed clear linear correlation between SOA and Ox in other megacities and other episodes. The lack of strong correlation between Ox and SOA usually implies that the timescale of SOA formation is longer since the timescale of Ox is approximately a few hours. Compared with well represented O_3 formation process in photochemical models, the significant uncertainties in the SOA predictions could be another reason for the non-linearity (Pun et al., 2003).

4. Conclusion

In this paper, O_3 were simulated in three week-long episodes in summer 2013 in China using modified WRF/CMAQ modeling system and anthropogenic emissions from MEIC. Model performance showed that WRF was reliable for providing meteorological inputs and the CMAQ generally reproduced O_3 concentrations all over China with missed peak values in some regions. Underestimation occurred at the June and July episodes in Central and South China while model performance was well acceptable in North, Northeast and East China. O_3 concentrations showed clear spatial and temporal variations. In August, the YRD and NCP both suffered extremely high O_3 concentrations (up to 100 ppb). NO_2, PAN and HNO_3 concentrations were higher at areas with high population density. HCHO concentration was higher in July and Central China. In severe O_3 polluted areas like NCP and YRD, OPR can be as high as 10 ppb/h in daytime, indicating a rapid increase in O_3 concentration. On the contrary, OPE was found to be as low as 2–4 in high NOx urban areas. O_3 isopleths showed that NOx control O_3 concentrations in most areas of China. Reducing VOCs has minor effects on O_3 concentrations while reducing NOx can largely reduce O_3 concentration except for areas such as Shanghai and Guangzhou. At last, linear correlations were found in August of Shanghai and Guangzhou between SOA and Ox concentrations with the slopes of 0.191 and 0.151 μg m^{-3} SOA/ppb Ox and R^2 values of 0.459 and 0.700, respectively. This correlation indicates that Ox and SOA may be produced

from similar sources and/or processes.

This study offers adequate and validated model performance all over China in summer episodes, and provides information on selecting controlling strategy towards O_3 concentration in China. The simulation results can be utilized to analyze O_3 formation in China in future research.

Acknowledgment

Portions of this research were conducted with high performance computing resources provided by Louisiana State University (http://www.hpc.lsu.edu). The project is funded by the Competitiveness Subprogram (RCS) from Louisiana Board of Regents (LEQSF(2016-19)-RD-A-14).

Appendix A. Supplementary data

Supplementary data to this article can be found online at https://doi.org/10.1016/j.apr.2019.05.003.

References

Borge, R., Alexandrov, V., Del Vas, J.J., Lumbreras, J., Rodriguez, E., 2008. A comprehensive sensitivity analysis of the WRF model for air quality applications over the Iberian Peninsula. Atmos. Environ. 42, 8560–8574.
Chan, C.K., Yao, X., 2008. Air pollution in mega cities in China. Atmos. Environ. 42, 1–42.
Cohan, D.S., Hakami, A., Hu, Y., Russell, A.G., 2005. Nonlinear response of ozone to Emissions: source apportionment and sensitivity analysis. Environ. Sci. Technol. 39, 6739–6748.
Crutzen, P.J., 1971. Ozone production rates in an oxygen-hydrogen-nitrogen oxide atmosphere. J. Geophys. Res. 76, 7311–7327.
Emery, C., Jung, J., Downey, N., Johnson, J., Jimenez, M., Yarwood, G., Morris, R., 2012. Regional and global modeling estimates of policy relevant background ozone over the United States. Atmos. Environ. 47, 206–217.
Emery, C., Tai, E., Yarwood, G., 2001. Enhanced Meteorological Modeling and Performance Evaluation for Two Texas Episodes. Report to the Texas Natural Resources Conservation Commission. prepared by ENVIRON. International Corp, Novato, CA.
Ervens, B., Volkamer, R., 2010. Glyoxal processing by aerosol multiphase chemistry: Towards a kinetic modeling framework of secondary organic aerosol formation in aqueous particles. Atmos. Chem. Phys. 10, 8219–8244.
Guenther, A., Jiang, X., Heald, C., Sakulyanontvittaya, T., Duhl, T., Emmons, L., Wang, X., 2012. The Model of Emissions of Gases and Aerosols from Nature Version 2.1 (MEGAN2. 1): An Extended and Updated Framework for Modeling Biogenic Emissions.
Guo, H., Wang, Y., Zhang, H., 2017. Characterization of criteria air pollutants in Beijing during 2014–2015. Environ. Res. 154, 334–344.
Hu, J., Chen, J., Ying, Q., Zhang, H., 2016. One-Year simulation of ozone and particulate matter in China using WRF/CMAQ modeling system. Atmos. Chem. Phys. 16, 10333.
Hu, J., Wang, Y., Ying, Q., Zhang, H., 2014. Spatial and temporal variability of PM2.5 and PM10 over the North China plain and the Yangtze River Delta, China. Atmos. Environ. 95, 598–609.
Jenkin, M.E., Clemitshaw, K.C., 2000. Ozone and other secondary photochemical pollutants: Chemical processes governing their formation in the planetary boundary layer. Atmos. Environ. 34, 2499–2527.
Jiang, W., Singleton, D.L., Hedley, M., McLaren, R., 1997. Sensitivity of ozone concentrations to VOC and NOx emissions in the Canadian lower Fraser Valley. Atmos. Environ. 31, 627–638.
Karambelas, A., Pye, H.O., Budisulistiorini, S.H., Surratt, J.D., Pinder, R.W., 2014. Contribution of isoprene epoxydiol to urban organic aerosol: Evidence from modeling and measurements. Environ. Sci. Technol. Lett. 1, 278–283.
Lei, Y., Zhang, Q., Nielsen, C., He, K., 2011. An inventory of primary air pollutants and CO_2 emissions from cement production in China, 1990–2020. Atmos. Environ. 45, 147–154.
Li, J., Cleveland, M., Ziemba, L.D., Griffin, R.J., Barsanti, K.C., Pankow, J.F., Ying, Q., 2015. Modeling regional secondary organic aerosol using the Master Chemical Mechanism. Atmos. Environ. 102, 52–61.
Li, M., Zhang, Q., Streets, D., He, K., Cheng, Y., Emmons, L., Huo, H., Kang, S., Lu, Z., Shao, M., 2014. Mapping Asian anthropogenic emissions of non-methane volatile organic compounds to multiple chemical mechanisms. Atmos. Chem. Phys. 14, 5617–5638.
Li, X., Rappenglück, B., 2014. A WRF–CMAQ study on spring time vertical ozone structure in Southeast Texas. Atmos. Environ. 97, 363–385.
Mai, J., Deng, T., Yu, L., Deng, X., Tan, H., Wang, S., Liu, X., 2016. A modeling study of impact of emission control strategies on PM2. 5 reductions in Zhongshan, China, using WRF-CMAQ. Adv. Meteorol. 2016.
MEP, 2012. China National Ambient Air Quality Standards. MEP, Beijing, China.
Mohan, M., Bhati, S., 2011. Analysis of WRF model performance over subtropical region of Delhi, India. Adv. Meteorol. 2011.
Paulot, F., Crounse, J.D., Kjaergaard, H.G., Kürten, A., Clair, J.M.S., Seinfeld, J.H., Wennberg, P.O., 2009. Unexpected epoxide formation in the gas-phase photooxidation of isoprene. Science 325, 730–733.
Pun, B.K., Wu, S.-Y., Seigneur, C., Seinfeld, J.H., Griffin, R.J., Pandis, S.N., 2003. Uncertainties in modeling secondary organic aerosols: Three-dimensional modeling studies in Nashville/Western Tennessee. Environ. Sci. Technol. 37, 3647–3661.
Shao, M., Zhang, Y., Zeng, L., Tang, X., Zhang, J., Zhong, L., Wang, B., 2009. Ground-level ozone in the Pearl River Delta and the roles of VOC and NOx in its production. J. Environ. Manag. 90, 512–518.
Sun, Y., Jiang, Q., Wang, Z., Fu, P., Li, J., Yang, T., Yin, Y., 2014. Investigation of the sources and evolution processes of severe haze pollution in Beijing in January 2013. J. Geophys. Res.: Atmosphere 119, 4380–4398.
Tonnesen, G.S., Dennis, R.L., 2000. Analysis of radical propagation efficiency to assess ozone sensitivity to hydrocarbons and NO x: 2. Long-lived species as indicators of ozone concentration sensitivity. J. Geophys. Res.: Atmosphere 105, 9227–9241.
Volkamer, R., San Martini, F., Molina, L.T., Salcedo, D., Jimenez, J.L., Molina, M.J., 2007. A missing sink for gas-phase glyoxal in Mexico City: Formation of secondary organic aerosol. Geophys. Res. Lett. 34.
Wang, S., Zhang, Q., Streets, D., He, K., Martin, R., Lamsal, L., Chen, D., Lei, Y., Lu, Z., 2012. Growth in NO x emissions from power plants in China: Bottom-up estimates and satellite observations. Atmos. Chem. Phys. 12, 4429–4447.
Wang, Y., Hu, B., Ji, D., Liu, Z., Tang, G., Xin, J., Zhang, H., Song, T., Wang, L., Gao, W., 2014a. Ozone weekend effects in the Beijing–Tianjin–Hebei metropolitan area, China. Atmos. Chem. Phys. 14, 2419–2429.
Wang, Y., Ying, Q., Hu, J., Zhang, H., 2014b. Spatial and temporal variations of six criteria air pollutants in 31 provincial capital cities in China during 2013–2014. Environ. Int. 73, 413–422.
Wei, W., Cheng, S., Li, G., Wang, G., Wang, H., 2014. Characteristics of ozone and ozone precursors (VOCs and NOx) around a petroleum refinery in Beijing, China. J. Environ. Sci. 26, 332–342.
Wen, L., Chen, J., Yang, L., Wang, X., Xu, C., Sui, X., Yao, L., Zhu, Y., Zhang, J., Zhu, T., 2015. Enhanced formation of fine particulate nitrate at a rural site on the North China Plain in summer: The important roles of ammonia and ozone. Atmos. Environ. 101, 294–302.
WHO, 2006. Air Quality Guidelines: Global Update 2005: Particulate Matter, Ozone, Nitrogen Dioxide, and Sulfur Dioxide. World Health Organization.
Wiedinmyer, C., Akagi, S., Yokelson, R.J., Emmons, L., Al-Saadi, J., Orlando, J., Soja, A., 2011. The Fire INventory from NCAR (FINN): A high resolution global model to estimate the emissions from open burning. Geosci. Model Dev. (GMD) 4, 625.
Wood, E., Canagaratna, M., Herndon, S., Onasch, T., Kolb, C., Worsnop, D., Kroll, J., Knighton, W., Seila, R., Zavala, M., 2010. Investigation of the correlation between odd oxygen and secondary organic aerosol in Mexico City and Houston. Atmos. Chem. Phys. 10, 8947–8968.
Ying, Q., Li, J., Kota, S.H., 2015. Significant contributions of isoprene to summertime secondary organic aerosol in eastern United States. Environ. Sci. Technol. 49, 7834–7842.
Zhang, H., Chen, G., Hu, J., Chen, S.-H., Wiedinmyer, C., Kleeman, M., Ying, Q., 2014. Evaluation of a seven-year air quality simulation using the Weather Research and Forecasting (WRF)/Community Multiscale Air Quality (CMAQ) models in the eastern United States. Sci. Total Environ. 473, 275–285.
Zhang, H., Ying, Q., 2011. Secondary organic aerosol formation and source apportionment in Southeast Texas. Atmos. Environ. 45, 3217–3227.
Zhao, B., Wang, S., Donahue, N.M., Jathar, S.H., Huang, X., Wu, W., Hao, J., Robinson, A.L., 2016. Quantifying the effect of organic aerosol aging and intermediate-volatility emissions on regional-scale aerosol pollution in China. Sci. Rep. 6.
Zheng, B., Huo, H., Zhang, Q., Yao, Z., Wang, X., Yang, X., Liu, H., He, K., 2014. High-resolution mapping of vehicle emissions in China in 2008. Atmos. Chem. Phys. 14, 9787–9805.